Modelling and Control of An Artificial Mouth of a Flute Wind Musical Instrument

Roy Abi Zeid Daou, Gaby Abou Haidar, Xavier Moreau

Modelling and Control of An Artificial Mouth of a Flute Wind Musical Instrument

Gaby ABOU HAIDAR
*Bordeaux University, CNRS, IMS Laboratory, CRONE Group
33600 Talence, Bordeaux, France
gabouhaidar@u-bordeaux.fr
* American University of Science and Technology, Faculty of Engineering
Zahle, Lebanon
gabouhaidar@aust.edu.lb

Roy ABI ZEID DAOU
* Lebanese German University, Biomedical technologies department,
Jounieh, Lebanon
r.abizeiddaou@lgu.edu.lb
* MART, Learning, Education and Training Center, Chananiir, Lebanon
roydaou@mart-ler.org

Xavier MOREAU
Bordeaux University, CNRS, IMS Laboratory, CRONE Group
33600 Talence, Bordeaux, France
Xavier.moreau@u-bordeaux.fr

***Abstract* — This paper focuses on the first step of a larger research program. The objective of this step is to model and control the initial part of a wind musical instrument (flute) which is the artificial mouth, for the purpose of precisely controlling the input pressure and the output flow that will be feeding the resonator of the instrument in order to get a very precise musical note. The modelling part will be done using Matlab/Simulink blocks that will present the system description and its parameters. The control law system design of the pressure inside the artificial mouth will be used in this modelling. For the control part, a frequency-domain approach is used to synthesize a traditional PI^2 controller and a CRONE controller. Finally, a comparative study shows that the CRONE controller leads to a better robust and stable degree of the pressure supply with respect to its uncertainties.**

***Keywords*- Wind musical instrument; pressure control; artificial mouth; CRONE controller; flute; PI^2 Controller.**

I. INTRODUCTION

Virtual modeling and construction of a musical instrument can afford to reproduce the exact sound of an existing instrument, even sounds that are unplayable in other parts of real physical instruments. Musical instruments are of different types: Beat, String, and wind instruments. The main focus here is a one type of wind musical instruments which is the flute. When modeling an acoustic tube, three principles must be kept in mind: Realism, low cost, and modularity. These three points are contradictory because for example, realism needs high cost. However, the main concept is the stability of the overall system in time and frequency domain. The three main parts of any wind instrument are the following: Mouth piece, resonator, and the horn or the radiator as seen in fig.1 [1].

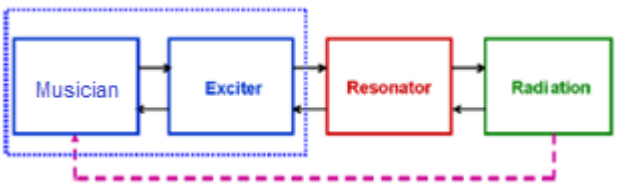

Fig. 1 Artificial loop based on the ear of the musician

Why developing a Model? Mainly to be able to play the flute numerically and precisely tune and control each musical note. In addition, modeling is a step towards optimizing the musical function of the flute and reduces error while playing music. Also this work will help beginners hear and play very accurate musical notes from their startup.

Blowing machines (so-called artificial mouths) were developed since the early stage of research in physical and musical acoustics for studying wind instruments [2] [3]. When replacing a musician by an artificial mouth, what is seeked is obviously more controlled measurements, since the different parameters may be tuned independently by the experimenter. In the past, the blowing pressure was generally manually adjusted using a pressure reducer, which became a delicate task when it was desired to obtain a precise blowing pressure, or even impossible when regular ramps were necessary to measure the bifurcations very precisely. This is the reason why the first artificial mouths were then equipped with pressure regulation based on PID controllers [2] [3].

The first step in this study is to develop a simulator programmed with Matlab/Simulink which will aid in the design of an artificial mouth. The second step will be the realization of the experimental model and its characteristics by comparing numerical simulation and experimentation results. The objective is then to complete and recalibrate the simulator so that it highly maps the experimental setup. The third step is the study of dynamic phenomena within the wind instrument both numerically and experimentally. These phenomena will be studied first from a point of view of the physical acoustics perspective, in particular the study of the viscothermic losses characterized by non-integer (or fractional) behaviors [4], then from a musical acoustics perspective.

Thus, this paper is divided into six sections. In section II, musical notes and their frequencies are presented. In section III, the general model of the flute instrument and its sub blocks are described with an emphasis on the first block e.g., the artificial mouth. In section IV, the process of modeling the artificial mouth is illustrated. Section V presents the control process of

the pressure at the artificial mouth using PI and CRONE controllers with their simulated results in frequency and time domains. Section VI concludes this paper with some proposed future work.

II. Musical Tones Description

Fig. 2 presents the different octaves, or doublings of the fundamental frequency, which are subdivided in twelve semitones. The frequency ratio between two semitones is constant and equal to $\sqrt[12]{2}$. The fundamental frequency of the middle (A=La) is set to 440 Hz in contemporary music [5].

	semitone	octave						
Do	C#	34.6	69.2	138.5	277.1	554.3	1108.7	2217.4
Re	D	36.7	73.4	146.8	293.6	587.3	1174.6	2349.3
Re	D#	38.8	77.7	155.5	311.1	622.2	1244.5	2489.0
Mi	E	41.2	82.4	164.8	329.6	659.2	1318.5	2637.0
Fa	F	43.6	87.3	174.6	349.2	698.4	1396.9	2793.8
Fa	F#	46.2	92.4	184.9	369.9	739.9	1479.9	2959.9
Sol	G	48.9	97.9	195.9	391.9	783.9	1567.9	3135.9
Sol	G#	51.9	103.8	207.6	415.3	830.6	1661.2	3322.4
La	A	55.0	110.0	220.0	**440.0**	880.0	1760.0	3520.0
La	A#	58.2	116.5	233.0	466.1	932.3	1864.6	3729.3
Si	B	61.7	123.4	246.9	493.8	987.7	1975.5	3951.0
Do	C	65.4	130.8	261.6	523.2	1046.5	2093.0	4186.0

Fig. 2. Musical notes with their corresponding frequencies

Equally tempered tuning will be used. Note that a musical instrument is tuned such that it approximates a system. For purely mechanical and constructional reasons, there are very few instruments that can be tuned exactly. Notable exceptions are the violin family, because here, the player is able to exactly determine the fundamental frequency of the note to be played. This is also the reason why there often exist different versions of the same instrument. For instance, flutes exist in contemporary and baroque tuning. It is important to define each musical note with its frequency. This will allow for high precision control and tuning [5].

III. Non Linear Modelling of Flute Artificial Mouth

Since the flute is composed mainly of three parts, we will focus now on modeling, controlling, and testing the mouth part by creating an artificial mouth and controlling its input and output pressure. For this reason, a physical setup was created to mimic the function of a flute. It is composed of a pressure source, pressure regulator, pressure sensor, servo-valve, flow sensor, artificial mouth, and the mouth piece of the flute.

Fig.3 shows the artificial mouth with its corresponding input pressure from a controlled servo valve. The servo valve is fed with compressed air about 6 bars which in turn is reduced by a pressure reducer. It is controlled by a computer system to achieve the most desirable output. The air flow from the output of the servo valve is measured via an air flow sensor for proper regulation of the air flowing into the artificial mouth. At the output of the artificial mouth, a pressure sensor is installed to read the output pressure which is read again via the computer system.

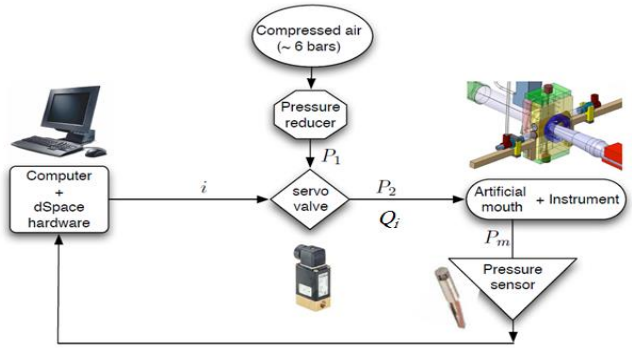

Fig. 3 Pressure controlled artificial mouth block diagram (see [3])

As shown in fig.3, the artificial mouth is the most critical part in this design since its input and output pressures must be highly controlled to produce the required frequency musical tone. Since our main focus at this stage is the artificial mouth modeling and control, we will start studying the transfer function characteristics of this part with respect to pressure.

The flow input and pressure output relation from the artificial mouth is presented in fig.4. The air flow is the controlled output of the servo valve with respect to the desired pressure at the artificial mouth output. This figure can be enlarged a represented as a block diagram as seen in fig.5.

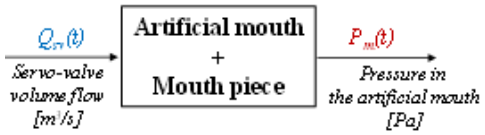

Fig. 4. Artificial Mouth Block input and output

Fig. 5 presents the block diagram of the nonlinear model of the artificial mouth with all the parameters related to flow, pressure, air density, surface area, volume, and the thermodynamic constants.

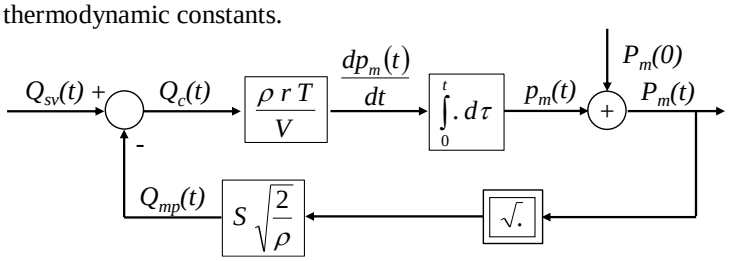

Fig. 5. Block diagram of the nonlinear model of the artificial mouth

Two different pressures can be observed in fig.3.The pressure $P_2(t)$ at the output of the servo-valve (input of the artificial mouth) and the pressure $P_m(t)$ measured inside the artificial mouth. These pressures are being compared to the atmospheric pressure P_{atm}.

The pressure drop in the components and the interconnections are defined as follow:

- pressure drop in the servo valve:

$$\Delta p_{sv}(t) = P_1 - P_2(t) \; ; \qquad (1)$$

- pressure drop in the servo valve artificial mouth connection pipe:

$$\Delta p_{pipe}(t) = P_2(t) - P_m(t)\ ; \qquad (2)$$

- pressure drop in the wind instrument mouth piece:

$$\Delta p_{mp}(t) = P_m(t) - P_{atm}\ . \qquad (3)$$

In this study, the servo valve and the artificial mouth are connected directly without any pipe, so one can consider that $\Delta p_{pipe}(t) = 0$ and so $P_2(t) = P_m(t)$.

Furthermore, these different pressures are linked by the relation:

$$\Delta p_{sv}(t) + \Delta p_{mp}(t) = P_1 - P_{atm} = \text{constant}\ , \qquad (4)$$

showing that if $\Delta p_{mp}(t)$ increases, then $\Delta p_{sv}(t)$ decreases, and reciprocally.

The artificial mouth is the central part that connects the volume flow $Q_{sv}(t)$ from the servo valve to the pressure $P_m(t)$ at the input of the mouth piece of the wind musical instrument. During the transient, dynamics induced by the filling of the mouth cavity has to be taken into account. Assuming air is a perfect gas, the state equation is given by:

$$P_m(t) = \frac{r\,T}{V}\,M(t)\,, \qquad (5)$$

where r represents the thermodynamic constant of air equal to 287 J.kg^{-1}.K^{-1}, T is the temperature of air at ambient conditions (equal to 293.5 K) and $M(t)$ is the mass of the air inside volume V (representing the artificial mouth). The mass $M(t)$ of air inside the cavity depends on the difference between the volume flow $Q_{sv}(t)$ at the input of the mouth and the volume flow $Q_{mp}(t)$ at the output (blown into the instrument). Since only small variations are considered, the air density ρ can be considered constant. In this case, the mass $M(t)$ is given by:

$$M(t) = \rho \int_0^t \left(Q_{sv}(\tau) - Q_{mp}(\tau)\right) d\tau + M(0)\,, \qquad (6)$$

where the expression of $Q_{mp}(t)$ is given by Bernoulli law:

$$Q_{mp}(t) = \alpha \sqrt{\Delta P_{mp}(t)}\ , \qquad (7)$$

with $\alpha = S\sqrt{\frac{2}{\rho}}$ and S the cross-section.

Fig.6 presents an example of time responses obtained with the simulator for the following scenario:

An analysis of the nonlinear model using the simulator allowed us to conclude that the amplitude of 0.1V of the harmonic signal $U_c(t)$ represents an upper bound of the small variations $u_c(t)$ around the operating point considered.

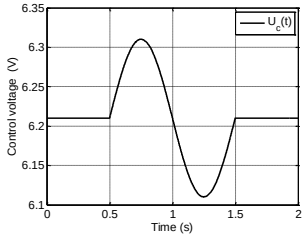

(a)

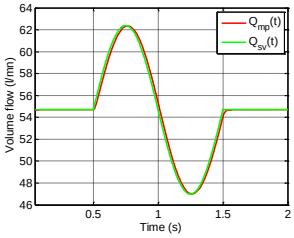

(b)

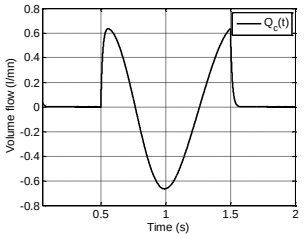

(c)

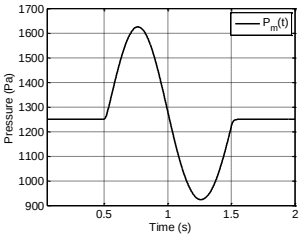

(d)

Fig. 6. Time responses of the nonlinear model: control voltage $U_c(t)$ (a), volume flow $Q_{sv}(t)$ and $Q_{mp}(t)$ (b), volume flow $Q_c(t)$ (c) and pressure $P_m(t)$ (d)

IV. Linearized Modelling of an Artificial Mouth

In order to linearize the model of the artificial mouth, the initial condition $P_m(0)$ is considered as an equilibrium pressure: $P_m(0) = P_m^e$. Therefore, $P_m(t)$ is defined as:

$$P_m(t) = P_m^e + p_m(t)\ , \qquad (8)$$

where $p_m(t)$ is a small variation around P_m^e.

As for the volume flow $Q_{mp}(t)$ inside the mouth piece:

$$Q_{mp}(t) = Q_{mp}^e + q_{mp}(t)\,, \qquad (9)$$

where $Q_{mp}^e = \alpha\sqrt{P_m^e}$ and $q_{mp}(t) = \frac{1}{R_{mp}}\,p_m(t)$, (10)

with $$\frac{1}{R_{mp}} = \left.\frac{\partial Q_{mp}}{\partial P_m}\right|_{P_m = P_m^e} = \frac{\alpha}{2\sqrt{P_m^e}}\ . \qquad (11)$$

Fig.8 presents the block diagram of the linearized model around the static equilibrium pressure P_m^e where C_{am} is the pneumatic capacity associated with the volume V of the artificial mouth: $C_{am}(s) = \frac{V}{\rho\,r\,T}$. (12)

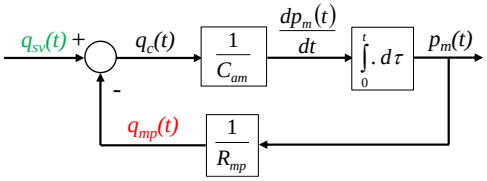

Fig.7 Block diagram of the linearized model of the artificial mouth

From the block diagram of fig.7, the transfer function $H_1(s)$ of the artificial mouth is deduced:

$$H_1(s) = \frac{\overline{P}_m(s)}{\overline{Q}_{sv}(s)} = \frac{R_{mp}}{1 + R_{mp}\,C_{am}\,s} = \frac{H_0}{1 + s/\omega_1}\,, \qquad (13)$$

where $H_0 = R_{mp}$, $\tau = R_{mp}\,C_{am}$ and $\omega_1 = 1/\tau$. (14)

The linearization of the servo-valve leads to a second order transfer function, $H_{sv}(s)$, defined by:

$$H_{sv}(s) = \frac{\overline{Q}_{sv}(s)}{\overline{U}_c(s)} = \frac{K_{sv}}{1 + 2\zeta\,\frac{s}{\omega_0} + \left(\frac{s}{\omega_0}\right)^2}\ . \qquad (15)$$

The complete linearized model used for the design of the control law is represented by the transfer function $G(s)$:

$$G(s)=\frac{\overline{P}_m(s)}{\overline{U}_c(s)}=\frac{G_0}{\left(1+\frac{s}{\omega_1}\right)\left(1+2\zeta\frac{s}{\omega_0}+\left(\frac{s}{\omega_0}\right)^2\right)}\quad,\qquad(16)$$

where $$G_0 = K_{sv}\,H_0\,.\qquad(17)$$

V. Control of Pressure at the Artificial Mouth Output with their Results

A. Values of the tested plant

In this paper, we consider that the supply pressure P_1 is uncertain. The different parameter values are:

$$\begin{cases} P_1 \in [3\,;6]\ \text{bar} \\ P_m^e = 1250\ \text{Pa} \\ S = 20\ \text{mm}^2 \\ V = 500\ \text{cm}^3 \\ T = 293.5\ \text{K} \end{cases} \text{ and } \begin{cases} G_0 \in [2011\,;3566]\ \text{Pa V}^{-1} \\ \omega_1 = 2\pi\ 12\ \text{rad/s} \end{cases}.\qquad(18)$$

For the control law, three transfer functions are defined:

$$\begin{cases} G_{min}(s) \text{ for } \underline{G_0} \\ G_{nom}(s) \text{ for } G_{0\_nom} = \left(\underline{G_0} + \overline{G_0}\right)/2 \end{cases} ; \quad G_{max}(s) \text{ for } \overline{G_0}\quad.\qquad(19)$$

Figure 8 presents the Bode plots of $G(j\omega)$ for three values of the supply pressure: P_1 = 3 bar (in blue), P_1 = 4.5 bar (in black) and P_1 = 6 bar (in red). It shows significant uncertainties on the gain whereas the phase is constant.

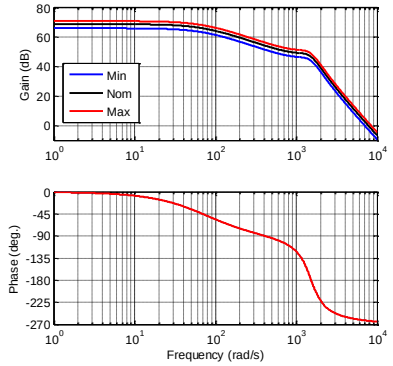

Fig. 8 Bode plots of $G(j\omega)$ for three values of the supply pressure: P_1 = 3 bar in blue, P_1 = 4.5 bar in black and P_1 = 6 bar in red

As for the linear feed forward, it is based on the inverse static gain of the linearized model used for the design of the control law, namely:

$$U_{ff}(t) = G_{0\_nom}^{-1}\ P_{ref}(t)\quad.\qquad(20)$$

B. User specifications

The user specifications of the control system defined from a preliminary work [1] [2] are the following:

- a phase margin $M_\Phi > 40°$;
- a open-loop gain crossover frequency ω_u = 63 rad/s;
- a steady-state error equal to 0 for a input ramp;
- a maximum of the variation ΔU of the control signal in the linear zone max[ΔU] = 1 V.

To have a significant comparison, the design of the two controllers PI² and CRONE is defined in order to obtain the same response speed, the same stability margins and the same precision in steady-state in the case of the nominal linearized model.

C. PI² Controller synthesis

For the nominal model, the user specifications can be respected by using a PI² controller. The frequency response for the PI² controller has the following form [11]:

$$C_{PI^2}(j\omega) = C_0\left(\frac{1+j\omega/\omega_i}{j\omega/\omega_i}\right)^2\quad.\qquad(21)$$

The parameter ω_i is defined referring to the first constraint of the user specifications as follows:

$$M_\Phi = \pi + \arg C_{PI^2}(j\omega_u) + \arg G_{nom}(j\omega_u),\qquad(22)$$

thus,
$$\omega_i = \frac{\omega_u}{\tan\left(\frac{M_\Phi - \arg G_{nom}(j\omega_u)}{2}\right)},\qquad(23)$$

where the notation "tan" is the trigonometric function *tangent*. C_0 is defined referring to the second constraint of the user specifications as follows:

$$\left|\beta(j\omega_u)\right| = C_0\left(\frac{1+(\omega_u/\omega_i)^2}{(\omega_u/\omega_i)^2}\right)\left|G_{nom}(j\omega_u)\right| = 1,\qquad(24)$$

where $\beta(j\omega)$ is the open-loop transfer function. Thus,

$$C_0 = \left(\left(\frac{1+(\omega_u/\omega_i)^2}{(\omega_u/\omega_i)^2}\right)\left|G_{nom}(j\omega_u)\right|\right)^{-1}\quad.\qquad(25)$$

With M_Φ = 45° and ω_u = 63 rad/s, we obtain:

$$\begin{cases} \omega_i = 66.5\ \text{rad/s} \\ C_0 = 2.24\ 10^{-4}\ \text{SI} \end{cases}.\qquad(26)$$

D. CRONE Control-System Design (CSD) methodology

The CRONE (a French acronym which means fractional order robust control) CSD methodology is a frequency-domain approach developed since the eighties [6] [7] [8] [9]. It is based on the common unity-feedback configuration to be presented later.

When the plant variations (due to plant parameter variations) are centered on frequency ω_u, the plant phase variation (with respect to the frequency) is cancelled by those of the controller. Then there is no phase margin variation when frequency ω_u varies. Such a controller produce a constant open loop phase whose Nichols locus is a vertical straight line named frequency template. This template ensures the robustness of phase and modulus margins and of resonant peaks of complementary sensitivity and sensitivity functions.

The general form of the nominal open-loop transfer function β_{nom}(s) of the second generation CRONE control is defined by equation (27):

$$\beta_{nom}(s) = \beta_0\left(\frac{1+s/\omega_l}{s/\omega_l}\right)^{n_l}\left(\frac{1+s/\omega_h}{1+s/\omega_l}\right)^{n}\left(1+s/\omega_h\right)^{-n_h}\quad.\qquad(27)$$

The first part of the above equation(30) represents the behavior at low frequencies with an integer order n_l, the second represents the behavior at middle frequencies with non-integer order n varying between 1 and 2 around ω_u, and the last represents the behavior at high frequencies with an integer order n_h. As for the gain β_0, it can be determined from the following relation [9]:

$$\beta_0 = (\omega_u/\omega_l)^{n_l}\left(1+(\omega_u/\omega_l)^2\right)^{(n-n_l)/2}\left(1+(\omega_u/\omega_h)^2\right)^{(n_h-n)/2}. \quad (28)$$

With $M_\Phi = 45°$, $\omega_u = 63$ rad/s, $G_0 \in [2011; 3566]$ Pa/V and in accordance with the methodology described in [9], we obtain the parameters of the open-loop transfer function:

$$\begin{cases} n_l = 2 \\ n = 1.5 \\ n_h = 4 \end{cases} \text{ and } \begin{cases} \omega_l = 3.46 \text{ rad/s} \\ \omega_h = 1141 \text{ rad/s} \\ \beta_0 = 70.22 \text{ SI} \end{cases}. \quad (29)$$

When the nominal open-loop transfer is determined, the fractional controller $C_F(s)$ is defined by its frequency response:

$$C_F(j\omega) = \beta_{nom}(j\omega)/G_{nom}(j\omega), \quad (30)$$

whose phase is variable. The synthesis of the rational controller $C_R(s)$ consists in identifying ideal frequency response $C_F(j\omega)$ by a of a low-order transfer function. The parameters of a transfer function with a predefined structure are adapted to frequency response $C_F(j\omega)$. The rational integer model on which the parametric estimation is based, is given by:

$$C_R(j\omega) = B(j\omega)/A(j\omega), \quad (31)$$

where $B(j\omega)$ and $A(j\omega)$ are polynomials of specified integer degrees n_B and n_A. All the frequency-domain system-identification techniques can be used.

From values given by equation (32), we obtain:

$$\begin{cases} B(s) = C_{R0}\prod_{i=1}^{6}\left(1+\frac{s}{\omega_{zi}}\right) \\ C_{R0} = 0.0254 \text{ SI} \\ A(s) = \left(\frac{s}{\omega_{p0}}\right)^2\prod_{j=1}^{5}\left(1+\frac{s}{\omega_{pj}}\right) \end{cases}, \quad (32)$$

with

	0	1	2	3	4	5	6
ω_{zi} (rad/s)		4.54	14.46	46.12	73.94	147	469
ω_{pj} (rad/s)	3.46	8.42	26.85	85.6	273	870	

Fig. 9 presents the Bode plots of the two controllers: $C_{PI2}(j\omega)$ (in blue) and $C_R(j\omega)$ (in black). One can observe that the two controllers have the same values of gain and phase at $\omega = \omega_u = 63$ rad/s.

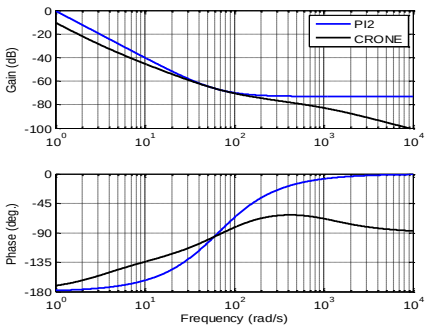

Fig. 9. Bode plots of $C_{PI2}(j\omega)$ (in blue) and $C_R(j\omega)$ (in black)

E. Results and testing

A- Fig.10 presents the structure of the Control Law System (CSL). The main function of the CSL is to satisfy robust tracking of the reference pressure $P_{ref}(t)$ of the artificial mouth. For this purpose, a control law system architecture presented below is designed. It consists of a robust controller synthesized with the CRONE methodology [6] [7] [8] allowing a control law by feedback pressure provided by a sensor system and a complementary control with a pressure feed forward.

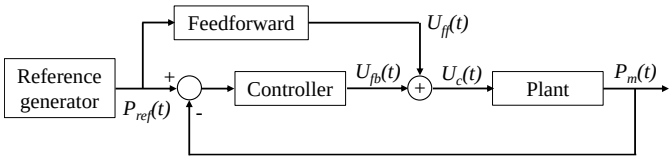

Fig. 10. Structure of the Control Law System (CSL)

B- Fig.11 presents the Nichols loci of $\beta(j\omega)$ obtained with the PI^2 controller (Fig.11.a) and the CRONE controller (Fig.11.b) for the three cases (min, nom, max). As one can see, for the nominal case (in black), the phase margin ($M_\Phi = 45°$) is the same with the two controllers. With the CRONE controller, the phase margin remains constant for all the cases (Fig.11.b), thus showing the robustness of the phase margin. It is not the case with the PI^2 controller (Fig.11.a).

Fig.12 presents the Bode plots of complementary sensitivity function $T(s)$ (a) (b), and sensitivity function $S(s)$ (c) (d) obtained with the PI^2 controller (a) (c) and the CRONE controller (b) (d) for the three cases (min, nom, max). For the nominal case (in black), the bandwidth at -3dB ($\omega_{3dB} = 100$ rad/s) and the resonant peak of $T(j\omega)$ ($Q_T = 3$dB) are the same with the two controllers. With the CRONE controller, the resonant peaks Q_T of $T(j\omega)$ (Fig.10.b) and Q_S of $S(j\omega)$ (Fig.12.d) remain constant for all the cases, thus showing the robustness of the resonant peaks. It is not the case with the PI^2 controller (Fig.12.a and c).

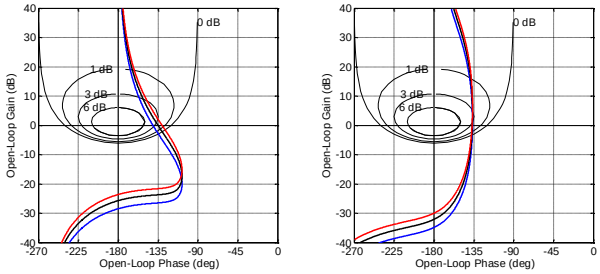

(a) (b)

Fig. 11. Nichols loci of $\beta(j\omega)$ obtained with the PI^2 controller (a) and the CRONE controller (b) for the three cases: min (in blue), nom (in black) and max (in red)

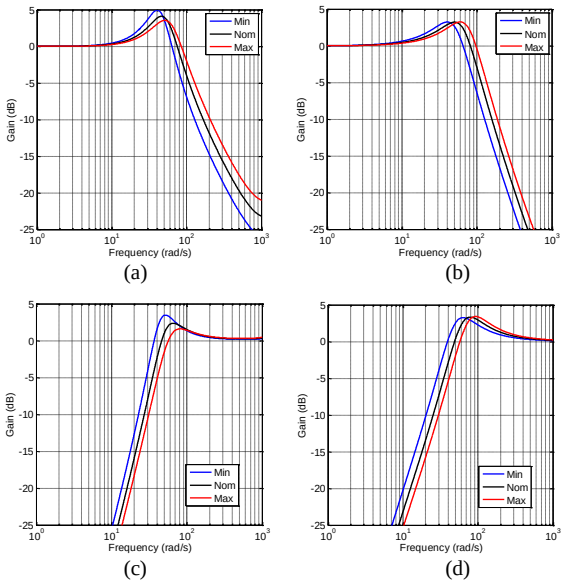

(a) (b)

(c) (d)

Fig. 12. Bode plots of $T(j\omega)$ (a) (b) and $S(j\omega)$ (c) (d) obtained with the PI^2 controller (a) (c) and the CRONE controller (b) (d) for the three cases: min, nom and max

Fig.13 presents the time responses of $p_m(t)$ (a) (b) and $u_c(t)$ (c) (d) obtained with the PI^2 controller (a) (c) and the CRONE controller (b) (d) applied to the nonlinear model (simulator) from a constant reference pressure P_{ref} = 1250 Pa, with a amplitude of the variation $p_{ref}(t)$ equals to 275 Pa (small variation) and for the three cases (min, nom, max). For the nominal case (in black), the rise time and the first overshoot (Fig. 13.a and b) of the small variation $p_m(t)$ are the same with the two controllers. With the CRONE controller, the first overshoot (Fig.13.b) remains constant for all the cases, thus showing the robustness of the stability degree.

As for the variation of the control signal $u_c(t)$ (Fig. 13.c and d), it is smaller than the maximum ΔU = 1 V in all the cases.

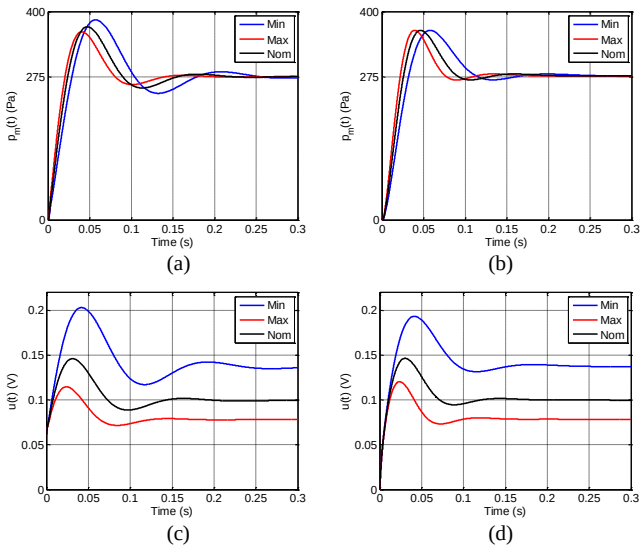

(a) (b)

(c) (d)

Fig. 13. Step responses of $P_m(t)$ (a) (b) and $U_c(t)$ (c) (d) obtained with: the PI^2 controller (a) (c) and the CRONE controller (b) (d) for P_1 = 3 bar in blue, P_1 = 4.5 bar in black and P_1 = 6 bar in red

VI. Conclusion and Future Works

A simulator programmed with MatLab/Simulink was developed and used to design a control law system of the pressure inside an artificial mouth. Simulation results show that CRONE CSD methodology leads to a better robustness of the stability degree with respect to uncertainties of the supply pressure in addition to a more tunable frequency of different musical notes.

The next step will be realizing the experimental model and its characteristics by comparing both numerical simulation and experimentation results. The objective will be to complete and recalibrate the simulator so that it is as faithful as possible to the experimental setup.

References

[1] B. De Moor R. Lauwereins, “Sound synthesis by simulation of physical models of musical instruments, U.D.C. 534.3 May 2003

[2] D. Ferrand and C. Vergez, ”Blowing machine for wind musical instrument: toward a real-time control of the blowing pressure”, 16th IEEE Mediterranean Conference on Control and Automation (MED), Ajaccio, France, 2008.

[3] D. Ferrand, C. Vergez , B. Fabre and F. Blanc, "High-precision regulation of a pressure controlled artificial mouth : the case of recorder-like musical instruments," *Acta Acustica united with Acustica, Hirzel Verlag,*, vol. 96, no. 4, pp. 701-712, 2010.

[5] D. Matignon and D. D’andréa-Novel, "Spectral and time-domain consequences of an integro-differential perturbation of the wave PDE," in *3rd WAVES conference*, Mandelieu, France, 1995.

[5] A. Chaigne “Modeling and simulation of musical instruments” Unit of Mechanical Engineering (UME), ENSTA ParisTech, Palaiseau, France

[6] A. Oustaloup, « La commande CRONE ». Hermes Editor, Paris. 1991.

[7] A. Oustaloup, La dérivation non entière : Théorie, synthèse et applications, Paris: Hermes, 1995.

[8] P. Lanusse, « De la commande CRONE de première génération à la commande CRONE de troisième generation ». PhD Thesis, Bordeaux I University, France, 1994.

[9] P. Lanusse, R. Malti and P. Melchior, "CRONE control system design toolbox for the control engineering community: tutorial and case study," *Philosophical transaction of the royal society*, vol. 391, pp. 1-14, 2013.

[10] A. Charef and N. Fergani, "PI$^\lambda$D$^\mu$ Controller Tuning For Desired Closed-Loop Response Using Impulse Response," in *Workshop on Fractional Derivation and Applications*, Spain, 2010.

[11] R. Abi Zeid Daou and X. Moreau, "A comparison between integer order and fractional order controllers applied to a hydro-electromechanical system," *Transaction on Control and Mechanical Systems*, vol. 2, no. 3, pp. 131-143, 2013.